NASA Technical Paper 2720

April 1987

Experimental Thrust Performance of a High-Area-Ratio Rocket Nozzle

Albert J. Pavli,
Kenneth J. Kacynski,
and Tamara A. Smith

NASA

NASA Technical Paper 2720

1987

Experimental Thrust Performance of a High-Area-Ratio Rocket Nozzle

Albert J. Pavli,
Kenneth J. Kacynski,
and Tamara A. Smith

Lewis Research Center
Cleveland, Ohio

National Aeronautics
and Space Administration

Scientific and Technical Information Branch

Summary

An experimental investigation was conducted to determine the thrust performance attainable from high-area-ratio rocket nozzles. A modified Rao-contoured nozzle with an expansion area ratio of 1030 was test fired with hydrogen-oxygen propellants at altitude conditions. The nozzle was also tested as a "truncated" nozzle, at an expansion area ratio of 428.

Thrust coefficient and thrust coefficient efficiency values are presented for each configuration at various propellant mixture ratios (oxygen/fuel). Several procedural techniques were developed that allowed improved measurement of nozzle performance. The more significant of these were (1) correcting the thrust for the aneroid effect, (2) determining the effective chamber pressure, and (3) referencing differential pressure transducers to a vacuum reference tank.

Introduction

The design of future space engines requires that many parameters be optimized to achieve the most effective configuration. The tradeoffs that must be made require the ability to predict the performance of components and systems as well as how the overall performance of the engine will vary with changes in these components and systems. Because of the large physical size of high-area-ratio nozzles, decisions can sometimes become clouded regarding the exact primary nozzle size, the size of extensions, and the materials needed to achieve the desired performance tradeoffs. The predictions of nozzle performance, especially at high expansion area ratios, do not have the accuracy needed. Furthermore the uncertainty is sufficiently large that meaningful tradeoffs cannot be made, and hence engine design points cannot be focused. The uncertainties result from a lack of knowledge of core flow, boundary layer interaction, contour effects, supersonic shock effects, wall heat transfer effects, and the specific impulse attainable from high-area-ratio nozzles. Data have been difficult to obtain because facilities are lacking for testing nozzles with area ratios in the range 700 to 1000, where theoretical design tradeoff studies are frequently quoted. No data at all are available above 400 and very limited data are published above 100.

Hence an experimental program was conducted to start obtaining some of these data. The tests were performed in the new altitude test capsule at the NASA Lewis Rocket Engine Test Facility. A contoured nozzle with a 2.54-cm (1-in.) diameter throat and an area ratio of 1030 was test fired with hydrogen-oxygen propellants, and the thrust performance was measured. This report presents the development of test procedural techniques and the first experimental data from this program.

Symbols

A_{ex}	nozzle exit area, m^2 ($in.^2$)
A_t	nozzle throat area, m^2 ($in.^2$)
A_v	venturi throat area, m^2 ($in.^2$)
C_d	venturi discharge coefficient, dimensionless
$C_{F,V}$	experimentally measured vacuum thrust coefficient, dimensionless
$C_{F,V,Th(ODE)}$	theoretical one-dimensional equilibrium (ODE) vacuum thrust coefficient, obtained from CEC program (ref. 1), dimensionless
$C_{F,V,Th(TDK)}$	theoretical two-dimensional kinetics vacuum thrust coefficient obtained from TDK program (ref. 2), dimensionless
C^*	experimentally measured characteristic exhaust velocity, m/sec (ft/sec)
C^*_{TH}	theoretical characteristic exhaust velocity, obtained from CEC program (ref. 1), m/sec (ft/sec)
F	experimentally measured thrust (corrected for aneroid effect), N (lb)
F_V	vacuum thrust (experimentally measured thrust corrected to vacuum conditions), N (lb)
g	gravitational constant, 9.807 m/sec^2 (32.174 ft/sec^2)
I	theoretical subsonic specific impulse inside combustion chamber, obtained from CEC program (ref. 1), sec
$I_{sp,V}$	experimentally measured vacuum specific impulse, sec
O/F	propellant mixture ratio, oxidizer flow divided by fuel flow, dimensionless
P_a	ambient static pressure around nozzle (altitude test capsule pressure), kN/m^2 (psia)

$P_{c,a}$	combustion chamber static pressure at injector end of combustion chamber, kN/m^2 (psia)
$P_{c,e}$	effective combustion chamber total pressure at nozzle entrance (integrated mean), kN/m^2 (psia)
$P_{c,T}$	combustion chamber total pressure after combustion ($P_{c,a}$ corrected for momentum pressure loss), kN/m^2 (psia)
P_{fi}	fuel injection pressure, kN/m^2 (psia)
P_{oi}	oxidizer injection pressure, kN/m^2 (psia)
P_s/P_T	static to total pressure ratio in combustion chamber (function of Mach number in combustion chamber), obtained from CEC program (ref. 1), dimensionless
T_{fi}	fuel injection temperature, K (°R)
T_{oi}	oxidizer injection temperature, K (°R)
V	velocity through venturi throat, m/sec (in./sec)
V_{av}	mass-averaged injection velocity of propellants, m/sec (ft/sec)
$\dot{W}$	propellant flow rate, kg/sec (lb/sec)
γ	ratio of specific heats, dimensionless
ϵ	nozzle expansion area ratio, dimensionless
ϵ_c	combustor contraction area ratio, dimensionless
η_{C^*}	characteristic exhaust velocity efficiency, percent
$\eta_{C_{F,V}}$	vacuum thrust coefficient efficiency, percent
$\eta_{I_{sp,V}}$	experimentally measured vacuum specific impulse efficiency (ratioed to ODE theoretical specific impulse derived from CEC program (ref. 1), percent
ρ	fluid density, kg/m^3 (lb/in.^{3})

Apparatus

Testing was done in the new altitude test capsule at the NASA Lewis Rocket Engine Test Facility (RETF) (fig. 1). Connecting the test capsule to the spray cooler is the water-jacketed second throat diffuser. The kinetic energy of the rocket exhaust gases is used in this diffuser to accomplish some of the altitude pumping of the test capsule. The diffuser was able to provide a pressure from 0.2 to 0.3 kN/m^2 (0.03 to 0.05 psia) in the test capsule while exhausting into the spray cooler, which was at 2 to 4 kN/m^2 (0.3 to 0.6 psia). The exhaust gases were pumped from the spray cooler by two means. Approximately half of the exhaust gases (products of hydrogen-oxygen combustion) were condensed to liquid water in the spray cooler. This water, along with the cooling spray water, exited the spray cooler through a vertical drain line down into the cylindrical detention tank shown on the valley floor next to the creek. This vertical drain line functioned as a barometric leg, allowing water to exit while preventing atmospheric air from entering the spray cooler. The other half of the exhaust gases (the noncondensables) were pumped out by the gaseous-nitrogen-driven ejectors shown mounted on top of the spray cooler. Four ejectors were connected in a series-parallel arrangement that provided two trains of two stages each. The exhaust from these ejectors was directed vertically upward through two short stacks and vented to the atmosphere.

The test capsule (fig. 2) was constructed in two parts. One part was the fixed end onto which the research hardware was mounted. The other part was the movable can, which could be rolled back to provide access to the experiment. Figure 2 shows the horizontal thrust stand with a test nozzle and a combustor installed onto the fixed end and the rest of the test capsule rolled back. The nozzle shown is the 1030-area-ratio nozzle with a flanged joint at the 428-area-ratio station. Mounted above the nozzle are the pressure transducers and valves to measure nozzle static pressure. Visible alongside the nozzle are some of the wall temperature thermocouples, in the process of being connected.

The instrumentation provided analog millivolt signals that were calibrated to be proportional to the magnitudes of the parameters to be measured. These analog signals were measured and converted to a digital signal by an automatic data digitizer at a rate of 50 readings per second per parameter and then sent to an IBM 370 computer. Once in the computer the millivolt values were converted to the engineering units of the measured parameters and averaged in groups of five readings. This provided data output at 1/10-sec intervals.

Two nozzles with 2.54-cm (1-in.) diameter throats were used in the work reported herein. One was a low-area-ratio design (ϵ = 1.4) for use at atmospheric pressure conditions. The other was an altitude nozzle with ϵ = 1030. The altitude nozzle was designed by the following procedure: Initially the Rao nozzle contour program (ref. 3) was run specifying certain properties including a ratio of specific heats γ of 1.23, a throat radius of 1.27 cm (0.5 in.), a chamber pressure of 6895 kN/m^2 (1000 psia), ϵ = 1000, and a nozzle length equivalent to 100 percent of a 15° cone. The Rao program uses the method of characteristics to calculate an optimum contour for an ideal-gas, constant-γ expansion. Next conditions within the Rao contour were predicted by using a one-dimensional kinetics analysis program (ref. 4). The input conditions to the kinetics program included a chamber pressure of 6895 kN/m^2 (1000 psia), a propellant mixture ratio of 6, a throat radius of 1.27 cm (0.5 in.), and hydrogen/oxygen combustion reactions. The one-dimensional kinetics program, developed at NASA Lewis, uses an implicit finite-difference technique to integrate the differential equations of chemical kinetics. Using the output from the kinetics program, the JANNAF boundary layer integral matrix procedure (BLIMP-J) (ref. 5) was then run to determine the characteristics of the boundary layer. BLIMP-J is a computer program that can compute the nonsimilar, chemically reacting laminar or turbulent boundary layer for nonablating

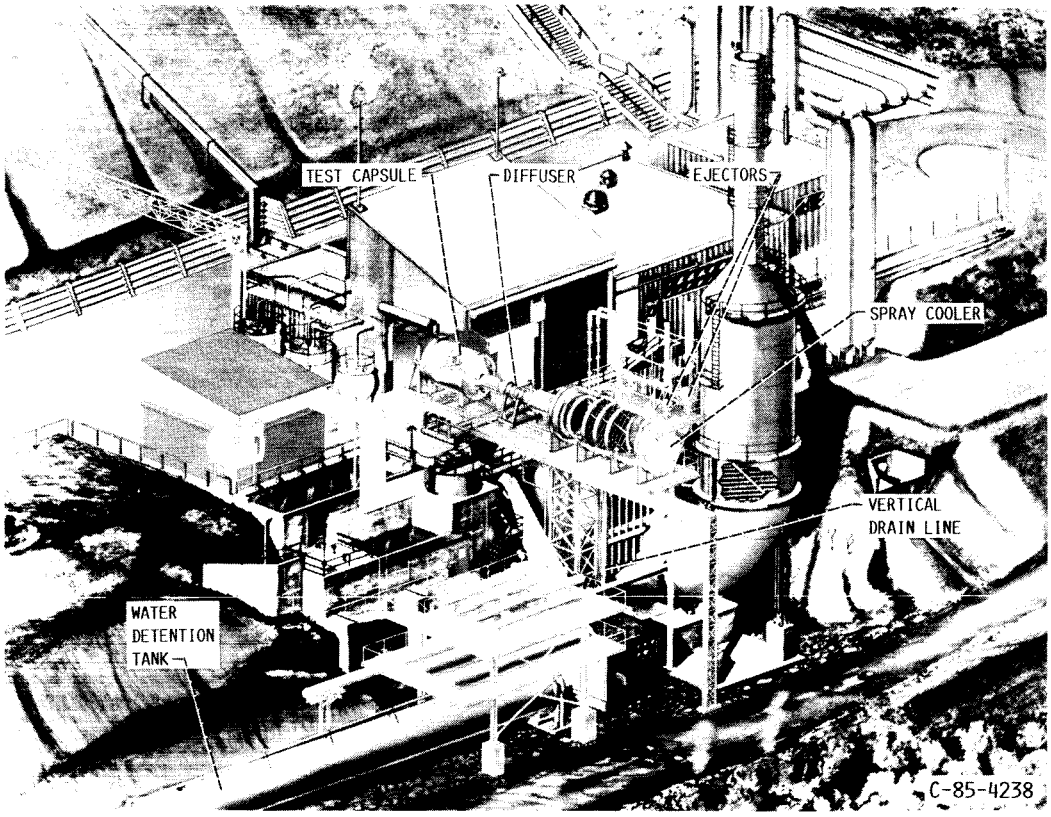

Figure 1.—NASA Lewis Rocket Engine Test Facility.

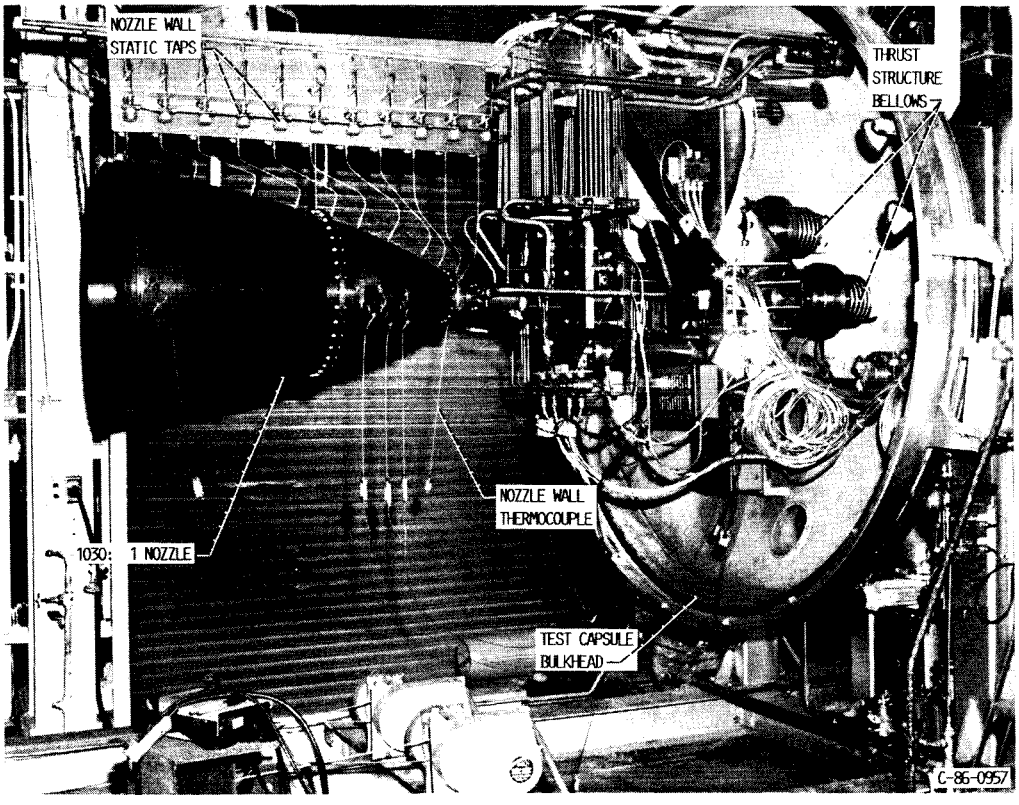

Figure 2.—Test capsule.

internal flow configurations. Aside from the properties calculated in the kinetics program for the 1000-area-ratio nozzle, an estimated inner wall axial temperature distribution was input to BLIMP-J. Other inputs to this program included the Cebeci-Smith turbulence model, the Buddenberg-Wilke mixture formula for viscosity, and the Mason-Saxena model with a Eucken correction for thermal conductivity. As an output the program estimated the displacement thickness of the boundary layer along the nozzle length. This displacement thickness was added onto the Rao contour at all stations along the flow axis. Thus a new contour was produced (fig. 3) that had an estimated "inviscid" core in the center with the boundary layer thickness added to the outside. This is the contour of the test nozzle. The nozzle was also tested in a truncated version by being disassembled at the 428-area-ratio joint, which occurred 63.147 cm (20.924 in.) from the throat.

Gaseous hydrogen and gaseous oxygen at ambient temperatures were supplied from high-pressure storage bottles and used as propellants for the combustor. The propellant system and the location of the instrumentation can be seen in figure 4. The propellant flow rates were measured by calibrated venturis and the temperatures were measured by thermocouples. The vacuum reference pressure was measured by a thermocouple vacuum gauge, and the rest of the pressures were measured by absolute or differential strain-gauge-bridge pressure transducers. The very low pressures from the static pressure taps on the nozzle wall and the test capsule altitude pressure were measured by the differential pressure transducers (ΔP). These units were then referenced to the vacuum reference pressure tank through a network of automatic shutoff and bypass valves. These transducers were ranged for only low values of differential pressure, namely 4 and 34 kN/m^2 (0.6 and 5.0 psi) full scale, and could not tolerate a differential pressure of 1 atmosphere across their diaphragms. However, because of their low ranges they were able to provide increased resolution in the measurement of these pressures.

The thrust stand could measure 13.3 kN (3000 lb) full scale and was attached to a foundation that was separate from the test capsule bulkhead. The thrust structure passed through the test capsule bulkhead by means of isolation ports that were sealed by metal bellows and was attached to the concrete floor outside the test capsule. The thrust stand was designed to have a 2σ variation of less than $\pm 1/10$ percent of full scale. The thrust stand could be calibrated remotely, in place, while at altitude, against an additional load cell. This load cell had a 2σ variation of less than ± 0.05 percent of full scale and a calibration traceable to the National Bureau of Standards.

The combustor used in this program (fig. 5) was uncooled and relied on its thermal inertia to survive the short firings (< 3 sec). Shown are the locations of two combustion chamber pressure taps. The two taps read essentially the same and were arithmetically averaged.

The injector used in this program (fig. 6) was a gaseous oxygen showerhead with the gaseous hydrogen flowing through the porous faceplate. It had 36 gaseous oxygen streams, arranged in a circular pattern. The igniter assembly, which also used gaseous hydrogen and gaseous oxygen as propellants, employed a spark plug as an ignition source and was located in the center of the injector. Once the desired chamber pressure was achieved in the combustor, the igniter oxygen flow was turned off while the hydrogen flow continued.

Axial distance from throat		Radius	
		cm	in.
cm	in.		
0	0	1.2700	0.5000
.3929	.1547	1.4371	.5658
.4641	.1827	1.4961	.5890
.6068	.2389	1.6190	.6374
.7503	.2954	1.7404	.6852
.8230	.3240	1.8031	.7099
1.3246	.5215	2.2426	.8829
1.7844	.7025	2.6515	1.0438
2.3777	.9361	3.1643	1.2458
3.2062	1.2623	4.2001	1.6536
7.0256	2.7660	6.6703	2.6261
7.8931	3.1075	7.2426	2.8514
9.6269	3.7901	8.3320	3.2803
10.6505	4.1931	8.9433	3.5210
11.6738	4.5960	9.5341	3.7536
12.9022	5.0796	10.2189	4.0232
15.3429	6.0405	11.5108	4.5318
16.5392	6.5115	12.1150	4.7697
19.5651	7.7028	13.5702	5.3426
23.3688	9.2003	15.2710	6.0122
25.4869	10.0342	16.1651	6.3642
29.5410	11.6303	17.7871	7.0028
33.7297	13.2794	19.3558	7.6204
36.2996	14.2912	20.2705	7.9805
38.8696	15.3030	21.1524	8.3277
41.4193	16.3068	21.9977	8.6605
47.2194	18.5903	23.8201	9.3780
51.1703	20.1458	24.9895	9.8384
55.1213	21.7013	26.1064	10.2781
60.4944	23.8167	27.5486	10.8459
71.1091	27.9957	30.1694	11.8777
76.2211	30.0083	31.3365	12.3372
90.6396	35.6849	34.3444	13.5214
105.3071	41.3532	36.9933	14.5643
113.0838	44.5212	38.3365	15.0931
128.5725	50.6191	40.6598	16.0078

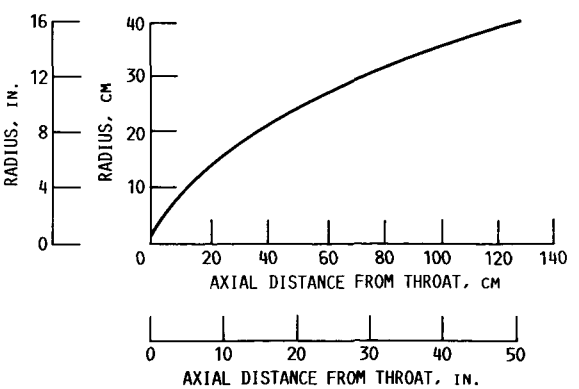

Figure 3.—Nozzle contour and coordinates.

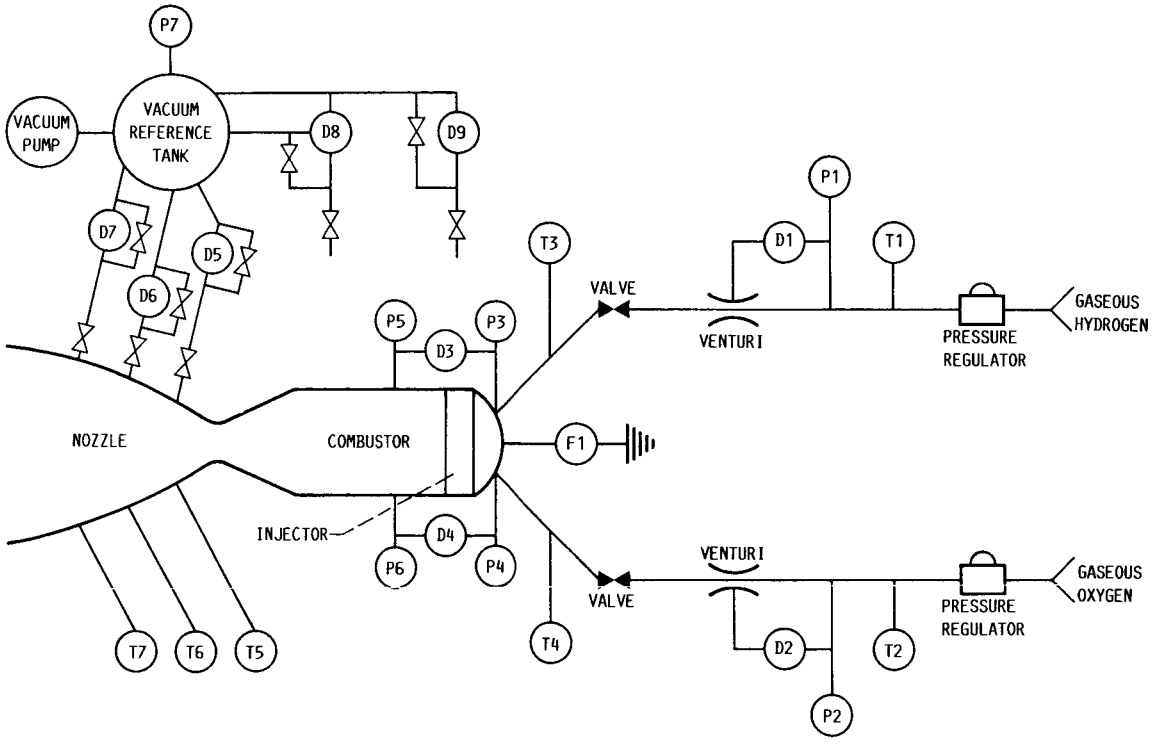

D1	FUEL VENTURI ΔP	D9	ALTITUDE ΔP
D2	OXYGEN VENTURI ΔP	F1	THRUST
D3	FUEL INJECTION ΔP	P1	FUEL SUPPLY PRESSURE
D4	OXYGEN INJECTION ΔP	P2	OXYGEN SUPPLY PRESSURE
D5	NOZZLE WALL ΔP	P3	FUEL INJECTION PRESSURE
D6	NOZZLE WALL ΔP	P4	OXYGEN INJECTION PRESSURE
D7	NOZZLE WALL ΔP	P5	CHAMBER PRESSURE
D8	ALTITUDE ΔP	P6	CHAMBER PRESSURE

P7	VACUUM REFERENCE PRESSURE	
T1	FUEL SUPPLY TEMPERATURE	
T2	OXYGEN SUPPLY TEMPERATURE	
T3	FUEL INJECTION TEMPERATURE	
T4	OXYGEN INJECTION TEMPERATURE	
T5	NOZZLE WALL TEMPERATURE	
T6	NOZZLE WALL TEMPERATURE	
T7	NOZZLE WALL TEMPERATURE	

Figure 4.—Schematic showing propellant system and instrumentation.

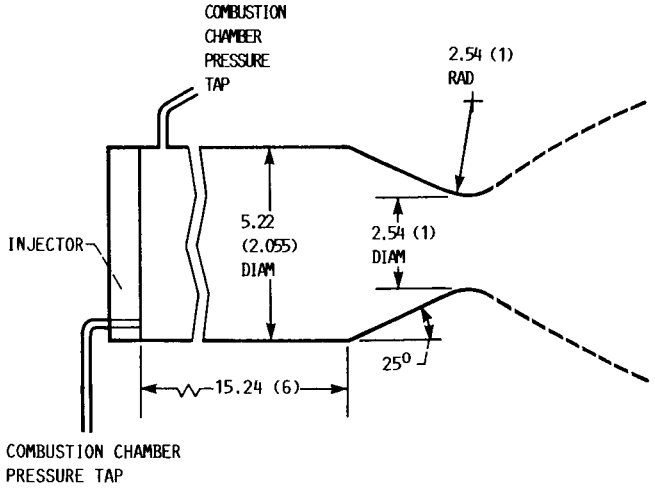

Figure 5.—Combustion chamber shape. For nozzle contour see figure 3. (Dimensions are in centimeters (inches).)

	Fuel	Oxygen
Number of holes	--------	36
Hole diameter, cm (in.)	--------	0.20 (0.078)
Nominal flow rate, $\dot{W}$, kg/sec (lb/sec)	0.102 (0.224)	0.432 (0.953)
Nominal pressure drop, ΔP, kN/m^2 (psi)	514.3 (74.6)	366.8 (53.2)

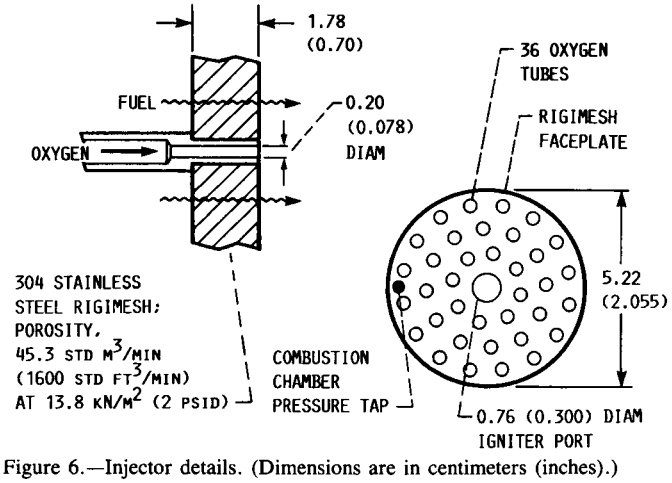

Figure 6.—Injector details. (Dimensions are in centimeters (inches).)

Procedure

Two types of tests were performed in this work: tests at atmospheric pressure conditions, and tests at altitude pressure conditions.

Atmospheric Pressure Tests

Atmospheric pressure tests were performed to determine the combustion efficiency and to otherwise characterize the injector. The test capsule can was rolled back out of the way, and the combustor was fired into the open air. The nozzle used in this testing was a heat-sink (uncooled) copper nozzle with a low expansion area ratio ($\epsilon = 1.4$). The firings were of approximately 3-sec duration.

Characteristic exhaust velocity and characteristic exhaust velocity efficiency were determined for the injector as a function of propellant mixture ratio O/F at a nominal chamber pressure of 2413 kN/m^2 (350 psia). Once the combustion losses were characterized, the nozzle performance evaluation was begun.

Altitude Tests

The nozzles had to be evaluated at altitude in order to run them at full flow, thereby precluding separated flow in the divergent portion of the nozzles. Although the thrust stand could measure the thrust at any altitude, it was found that the zero thrust reading changed as a function of the altitude pressure. If the test capsule had been at a constant altitude pressure before, during, and after the firing, there would have been no change in the zero thrust reading. However, the desired altitude pressure was achieved only after the thruster fired, since a considerable amount of altitude pumping was accomplished by the exhaust gases in the diffuser. This resulted in a zero shift in the thrust measurement during the firing. It was found that an aneroid force on the hermetically sealed load cells was responsible for this zero shift. This effect was calibrated (fig. 7) by pumping the test capsule to a low pressure with a mechanical pump while reading the thrust stand zero value. A straight line was faired through the data from each of the two test capsule pressure transducers used in this calibration. A discrepancy of approximately 1.4 kN/m^2 (0.2 psi) is apparent. This discrepancy does not affect the slope of the data, which is the main concern. The slope of the data is equivalent to an aneroid force acting on an effective surface area of 27.774 cm^2 (4.305 in.^{2}) in a negative direction. This aneroid force thrust correction has been applied to all the data reported herein.

A typical altitude firing would start with the gaseous nitrogen ejectors evacuating the test capsule and the spray cooler to a pressure of approximately 2 to 4 kN/m^2 (0.3 to 0.6 psia). Then the thruster would be test fired for the nominal duration of 3 sec. During this time the exhaust gases would entrain some of the remaining gases in the test capsule and carry them through the diffuser into the spray cooler. This pumping action would further depress the pressure in the test capsule from 2 to 4 kN/m^2 (0.3 to 0.6 psia) to 0.2 to 0.3 kN/m^2 (0.03 to 0.05 psia). A steady-state pressure condition would be achieved at or before 2½ sec, allowing about 1/2 sec of steady-state data to be obtained before shutdown.

At thruster shutdown the exhaust flow through the diffuser would stop, and a pressure pulse would backflow from the spray cooler into the test capsule, raising the test capsule pressure back to the original 2 to 4 kN/m^2 (0.3 to 0.6 psia). No problem was encountered in tolerating this pressure pulse.

At this time two isolation valves between the ejectors and the spray cooler would close, and the gaseous nitrogen to the ejectors would be turned off. The pressure in the test capsule would then be slowly raised to atmospheric pressure by bleeding in air through a small valve.

Data Analysis

Flow measurement. – Venturis were used in measuring the primary propellant weight flows. Each weight flow was found by determining conditions at the venturi throat:

$$\dot{W} = C_d \rho A_v V \tag{1}$$

Throat density and velocity were calculated by using one-dimensional mass and energy equations and assuming real-gas behavior. The fluid properties program, GASP (ref. 6), was used in determining all necessary properties. Venturi calibrations were performed by the Colorado Engineering Experiment Station. Values of the discharge coefficient are traceable to the National Bureau of Standards, and the uncertainty values are ±0.5 percent.

The igniter flow (fuel only) was left on during all testing. This flow amounted to less than 0.4 percent of the total propellant weight flow. The igniter weight flow was calculated by assuming ideal-gas flow and then added to the injector flow to obtain the total propellant flow.

Thrust measurement. – As discussed previously, an aneroid corrective term was added to account for the transient nature of the capsule pressure during a test firing. This caused the sensitive portion of the load cell to experience a time-varying pressure difference. The result is equivalent to a time-(pressure) dependent zero thrust variation. Appropriate calibrations (fig. 7) for this effect were performed and are accounted for in the data analysis.

Vacuum thrust was determined by adding the product of the capsule pressure (absolute) and the nozzle exit area to the measured thrust. That is,

$$F_V = F + \left(P_a \times A_{ex}\right) \tag{2}$$

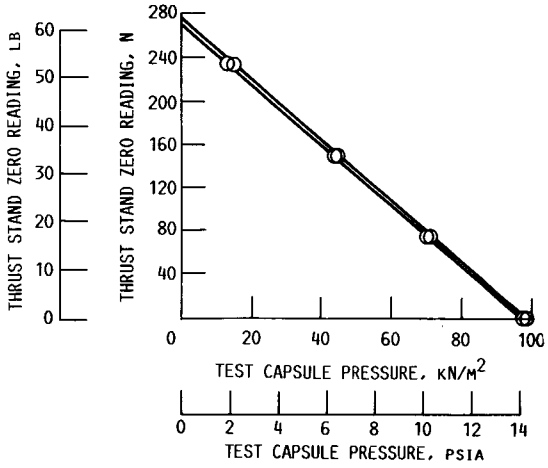

Figure 7.—Aneroid force correction.

Theoretical Performance

Theoretical rocket performance values were calculated by using the Chemical Equilibrium Composition (CEC) program (ref. 1). Inlet enthalpy conditions were determined by measuring fuel and oxygen injection pressure and temperature.

Throat Total Pressure Calculations

Nozzle throat total pressure was determined by two means. The first method was to measure chamber pressure at the injector end and correct it to the total pressure within the chamber after combustion

$$P_{c,T} = P_{c,a}\left[\frac{P_s}{P_T} + \frac{Ig - V_{av}}{C^*_{TH}\epsilon_c}\right]^{-1} \tag{3}$$

which is the momentum pressure loss equation (ref. 7).

The mass-averaged velocity V_{av} was calculated by measuring the injector pressure drops and assuming an effective fuel and oxygen injection area. All other terms were calculated by using the CEC program (ref. 1). For the high combustor contraction ratios ϵ_c used in this program the momentum pressure loss term is near unity (~ 0.993).

The second method was to calculate an effective pressure $P_{c,e}$ from vacuum thrust measurements and predicted vacuum thrust coefficients. This procedure was used for the low-area-ratio ($\epsilon = 1.4$) tests only.

$$P_{c,e} = \frac{F_V}{C_{F,V,\mathrm{Th(TDK)}}A_t} \tag{4}$$

Vacuum thrust coefficient predictions for the 1.4-area-ratio nozzle were performed using the December 1984 revised Two-Dimensional Kinetics (TDK) program (ref. 2). Options used in the program were equilibrium expansion, cone divergence, and laminar boundary layer flow. The wall temperature profile was estimated by assuming transient, one-dimensional (radial) heat transfer. Heat transfer coefficients were calculated as a function of nozzle contraction (and expansion) area ratio. As frictional drag is relatively small at low area ratios, wall temperature has very little effect on the overall thrust coefficient.

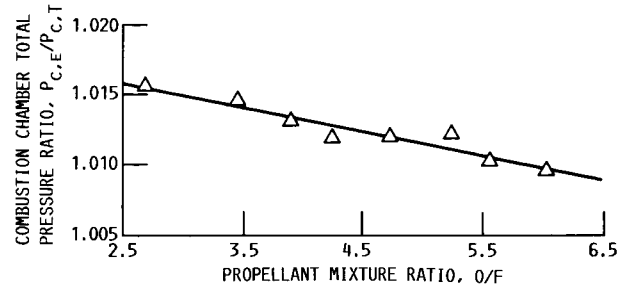

Figure 8.—Effective chamber pressure correlation.

Historically, circumferential and radial pressure distributions have been known to exist at the injector face. Therefore discrete pressure measurements at the injector face may not truly represent an overall (average) chamber pressure. What is needed is an integrated mean of the pressure distribution across the whole injector face. The effective combustion chamber total pressure $P_{c,e}$ described above is such an integrated mean. Therefore it was decided that for the low-area-ratio tests $P_{c,e}$ was more accurate than $P_{c,T}$. And furthermore that for the high-area-ratio nozzle tests $P_{c,e}$ would be determined by measuring injector-end static pressure $P_{c,a}$, correcting it for momentum pressure loss to obtain $P_{c,T}$, and then multiplying it by the ratio $P_{c,e}/P_{c,T}$ obtained in the low-area-ratio (atmospheric) tests. The ratio $P_{c,e}/P_{c,T}$ versus O/F for the low-area-ratio tests is presented in figure 8. The line of best fit (least-squares method) presented in this figure represents the correction ratio that was applied during the high-area-ratio tests.

Performance Calculations

By definition

$$C^* = \frac{P_{c,e}A_t g}{\dot{W}} \tag{5}$$

$$C_{F,V} = \frac{F_V}{P_{c,e}A_t} \tag{6}$$

$$I_{sp,V} = \frac{F_V}{\dot{W}} \tag{7}$$

The values of $P_{c,e}$ were determined as described in the

preceding section. Weight flow and vacuum thrust calculations are also described in previous sections. Throat area was determined daily from measurements of the throat diameter. Localized throat erosion was observed after testing the 1030- and 428-area-ratio configurations. The total change in geometric throat area was approximately 0.03 percent. No data corrections were made to account for the erosion.

Efficiency Calculations

All of the performance parameters ($I_{sp,V}$, $C_{F,V}$, C^*) were compared with theoretical one-dimensional equilibrium (ODE) rocket performance values by using the CEC program (ref. 1). Values of the theoretical vacuum thrust coefficient efficiency $\eta_{C_{F,V}}$ are presented for the low-area-ratio nozzle tests in table I. These values represent predictions obtained from the Two-Dimensional Kinetics (TDK) program. The options used for the TDK program were equilibrium expansion, cone divergence, and laminar boundary layer flow.

Results and Discussion

Atmospheric Pressure Tests

Atmospheric pressure tests were performed to characterize the injector and to determine the combustion losses. The results of eight test firings are summarized in table I. The effective chamber pressure $P_{c,e}$ was approximately 1 percent higher than the measured chamber pressure $P_{c,T}$, probably because of local pressure variations. We felt that $P_{c,e}$ more accurately represented the actual pressure at the nozzle entrance than did the measurement from a simple static pressure tap that was subject to local variations. Therefore we developed a correlation between the effective and measured chamber pressures. The $P_{c,e}/P_{c,T}$ values (given in table I) formed the basis for determining the effective chamber pressure to be used in processing the altitude test data.

The effective chamber pressure correction $P_{c,e}/P_{c,T}$ seemed to correlate with the mixture ratio O/F (fig. 8). A straight line through the data was used to correlate the data, and then

TABLE I.—RESULTS OF ATMOSPHERIC PRESSURE TESTS

[Ambient pressure around nozzle, P_a, 98 kN/m² (14.214 psia).]

Reading	Measured chamber pressure at injector end of chamber, $P_{c,a}$		Measured chamber pressure corrected for momentum pressure loss, $P_{c,T}$		Propellant mixture ratio, O/F	Measured thrust (corrected for aneroid effect), F		Vacuum thrust, measured thrust corrected to vacuum conditions, F_V		Propellant flow rate, $\dot{W}$		Fuel injection pressure, P_{fi}		Fuel injection temperature, T_{fi}	
						N	lb			kg/sec	lb/sec				
	kN/m²	psia	kN/m²	psia				N	lb			kN/m²	psia	K	°R
98	2435	353.2	2426	351.8	3.89	1587	356.7	1657	372.5	0.5116	1.128	2992	434.0	287.1	516.7
99	2510	364.0	2500	362.7	4.24	1635	367.6	1705	383.3	.5343	1.178	3024	438.6	286.7	516.0
100	2347	340.4	2335	338.6	2.69	1532	344.4	1602	360.1	.4813	1.061	3181	461.4	286.4	515.5
101	2493	361.6	2487	360.7	5.24	1623	364.8	1693	380.6	.5498	1.212	2897	420.1	286.4	515.6
104	2482	360.0	2478	359.4	6.03	1615	363.1	1685	378.8	.5647	1.245	2826	409.9	286.1	515.0
105	2470	358.2	2462	357.1	4.72	1608	361.5	1678	377.2	.5361	1.182	2919	423.3	286.1	514.9
106	2483	360.1	2478	359.4	5.56	1615	363.0	1685	378.7	.5602	1.235	2863	415.3	286.5	515.7
107	2370	343.8	2359	342.2	3.45	1545	347.4	1615	363.1	.4921	1.085	2992	434.0	286.0	514.8

Reading	Oxidizer injection pressure, P_{oi}		Oxidizer injection temperature, T_{oi}		Theoretically predicted			Effective chamber total pressure calculated from thrust, $P_{c,e}$		Correlation pressure ratio for use in altitude tests, $P_{c,e}/P_{c,T}$	Characteristic exhaust velocity efficiency, η_{C^*}, percent	Vacuum specific impulse, $I_{sp,V}$, sec	Vacuum specific impulse efficiency, $\eta_{I_{sp,V}}$, percent
					ODE vacuum thrust coefficient, $C_{F,V,Th(ODE)}$	TDK vacuum thrust coefficient, $C_{F,V,Th(TDK)}$	Vacuum thrust coefficient efficiency, TDK/ODE, $\eta_{C_{F,V}}$						
	kN/m²	psia	K	°R				kN/m²	psia				
98	2770	401.8	285.6	514.0	1.370	1.336	97.5	2457	356.4	1.013	96.5	330.1	94.1
99	2877	417.2	285.2	513.3	1.370	1.335	97.5	2530	367.0	1.012	96.1	325.5	93.7
100	2587	375.2	285.8	514.4	1.373	1.339	97.5	2371	343.9	1.016	97.3	339.6	94.9
101	2918	423.2	284.9	512.8	1.369	1.332	97.3	2518	365.2	1.012	96.1	314.0	93.5
104	2948	427.5	283.9	511.1	1.369	1.335	97.5	2501	362.8	1.010	95.8	304.2	93.4
105	2860	414.8	284.9	512.9	1.369	1.334	97.4	2492	361.4	1.012	95.8	319.2	93.4
106	2920	423.5	284.7	512.5	1.369	1.334	97.4	2504	363.1	1.010	94.9	306.8	92.5
107	2668	387.0	285.1	513.1	1.370	1.337	97.5	2394	347.2	1.015	96.8	334.6	94.4

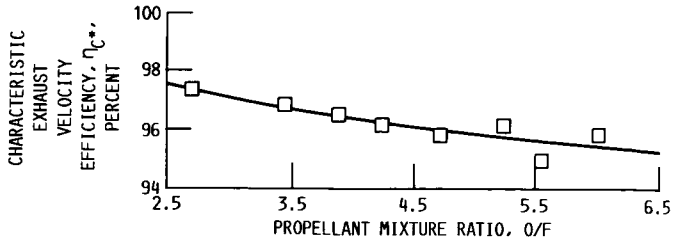

Figure 9.—Injector combustion performance at atmospheric pressure. Expansion area ratio, $\epsilon = 1.4$. (Efficiency is based on ODE program.)

this linear relationship was used to obtain values of $P_{c,e}$ from chamber pressures measured in the high-area-ratio nozzle tests.

The combustion performance of the injector determined from the eight atmospheric pressure test firings is shown in figure 9.

Altitude Tests

Thirteen successful altitude firings were accomplished, 11 with the full 1030-area-ratio nozzle, and two with the nozzle truncated to $\epsilon = 428$. The results of these firings are summarized in table II. The effective chamber pressure correction $P_{c,e}$ compensates for the effect of static pressure profiles in the combustor and is in effect a calibration of the chamber-pressure static pressure tap.

The measured vacuum thrust coefficient and the vacuum thrust coefficient efficiency for the 1030-area-ratio nozzle varied as a function of the propellant mixture ratio (fig. 10) A similar dependence on mixture ratio was observed in the data for the truncated ($\epsilon = 428$) nozzle (fig. 11). Although there are only two data points to report, the line through these data points closely parallels the data trends shown in the high-area-ratio tests.

TABLE II.—RESULTS OF ALTITUDE TESTS

Reading	Nozzle exit expansion area ratio, ϵ	Measured chamber pressure at injector end, $P_{c,a}$		Chamber pressure corrected for momentum pressure loss, $P_{c,T}$		Effective chamber pressure calculated with low ϵ correlation, $P_{c,e}$		Propellant mixture ratio, O/F	Fuel injection pressure, P_{fi}		Fuel injection temperature, T_{fi}		Oxidizer injection pressure, P_{oi}	
		kN/m^2	psia	kN/m^2	psia	kN/m^2	psia		kN/m^2	psia	K	°R	kN/m^2	psia
112	1030	2459	356.7	2449	355.2	2482	360.0	3.84	3061	444.0	285.6	514.1	2809	407.4
113		2439	353.7	2430	352.4	2461	356.9	4.36	2956	428.8	284.2	511.5	2818	408.7
114		2467	357.8	2460	356.8	2488	360.9	5.08	2912	422.4	283.9	511.1	2890	419.2
115		2429	352.3	2423	351.4	2450	355.3	5.49	2843	412.4	283.5	510.3	2870	416.3
116		2459	356.6	2445	354.6	2482	360.0	2.85	3284	476.3	281.5	506.7	2742	397.7
117		2433	352.9	2421	351.1	2456	356.2	3.19	3160	458.3	281.1	506.0	2735	396.7
120		2427	352.0	2418	350.7	2449	355.2	4.30	2950	427.8	294.4	529.9	2803	406.6
121		2460	356.8	2450	355.4	2482	360.0	4.11	3013	437.0	295.0	531.0	2832	410.7
123		2426	351.9	2414	350.1	2449	355.2	3.19	3152	457.2	295.6	532.0	2732	396.2
124		2468	358.0	2455	356.0	2492	361.4	2.78	3328	482.7	295.9	532.6	2752	399.1
125		2418	350.7	2408	349.2	2441	354.0	3.74	3028	439.1	296.3	533.3	2763	400.7
136	428	2361	342.4	2353	341.2	2383	345.6	3.04	3123	452.9	292.1	525.7	2648	384.1
137	428	2435	353.1	2426	351.8	2457	356.8	4.29	2965	430.0	291.2	524.2	2813	408.0

Reading	Oxidizer injection temperature, T_{oi}		Propellant flow rate, $\dot{W}$		Vacuum thrust, F_V		Ambient pressure around nozzle, P_a		Characteristic exhaust velocity, C^*		Characteristic exhaust velocity efficiency, η_{C^*}, percent	Measured vacuum thrust coefficient, $C_{F,V}$	Thrust coefficient efficiency, $\eta_{C_{F,V}}$, percent	Vacuum specific impulse $I_{sp,V}$, sec	Vacuum specific impulse efficiency, $\eta_{I_{sp,V}}$, percent
	K	°R	kg/sec	lb/sec	N	lb	kN/m^2	psia	m/sec	ft/sec					
112	502.5	279.2	0.5266	1.161	2422	544.4	0.2682	0.0389	2402	7880	95.5	1.917	97.3	468.9	92.9
113	498.6	277.0	.5334	1.176	2409	541.6	.2592	.0376	2346	7697	95.0	1.914	95.3	460.4	90.5
114	496.4	275.8	.5543	1.222	2457	552.3	.2530	.0367	2283	7491	94.4	1.941	94.0	451.9	88.8
115	496.6	275.9	.5552	1.224	2448	550.4	.2530	.0367	2244	7363	94.2	1.967	93.7	449.7	88.3
116	496.4	275.8	.5094	1.123	2362	531.0	.2965	.0430	2479	8134	97.2	1.871	98.4	473.0	95.6
117	495.2	275.1	.5094	1.123	2364	531.5	.2461	.0357	2453	8048	96.4	1.892	98.4	473.4	94.9
120	517.5	287.5	.5316	1.172	2429	546.1	.2544	.0369	2377	7799	95.7	1.923	96.0	466.1	91.8
121	518.9	288.3	.5293	1.167	2459	552.9	.2654	.0385	2418	7934	96.8	1.921	96.6	473.6	93.5
123	521.0	289.4	.5039	1.111	2377	534.3	.2592	.0376	2508	8228	98.4	1.881	97.7	481.1	96.2
124	521.1	289.5	.5058	1.115	2386	536.4	.2441	.0354	2543	8342	99.4	1.857	97.8	481.3	97.3
125	520.6	289.2	.5135	1.132	2406	541.0	.2420	.0351	2451	8042	97.2	1.912	97.4	477.8	94.6
136	517.7	287.6	.4917	1.084	2228	500.9	.3916	.0568	2487	8158	97.4	1.823	96.0	462.3	93.6
137	513.0	285.0	.5330	1.175	2365	531.6	.3916	.0568	2364	7757	95.2	1.877	94.8	452.6	90.2

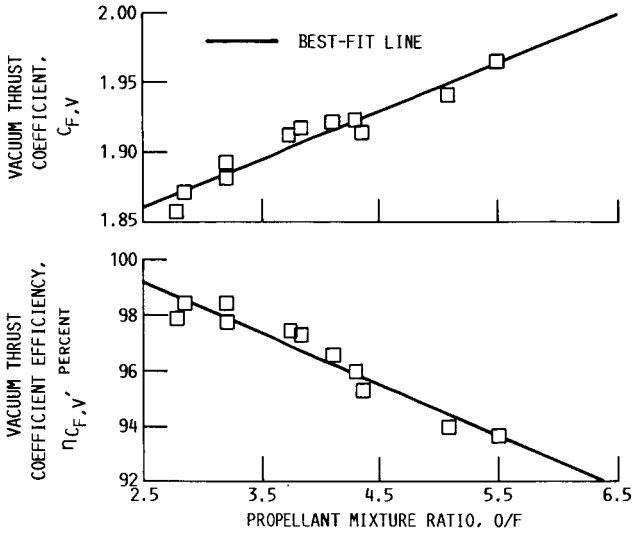

Figure 10.—Vacuum thrust performance of 1030-area-ratio nozzle. (Efficiency is based on ODE program.)

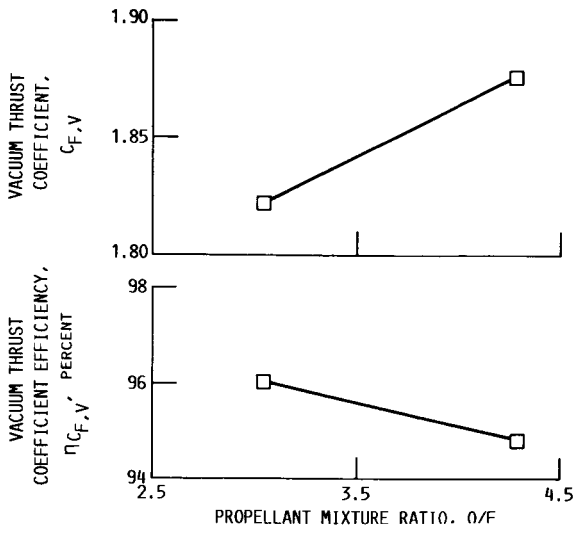

Figure 11.—Vacuum thrust performance of 428-area-ratio nozzle. (Efficiency is based on ODE program.)

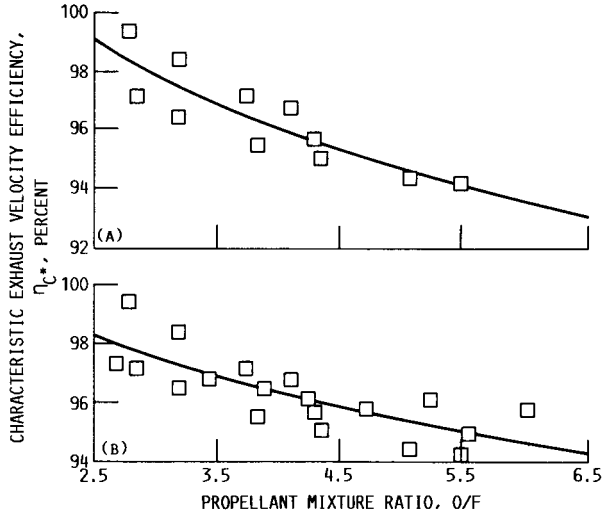

(a) Altitude tests.
(b) Atmospheric and altitude data combined.

Figure 12.—Injector combustion performance at altitude.

The characteristic exhaust velocity efficiency from the altitude tests agreed well with data from the atmospheric tests (fig. 12).

The nozzle wall static pressures were measured at 11 area ratio locations (table III). The last static pressure tap before the nozzle exit was at $\epsilon = 975$. In all cases except one, the static pressure at $\epsilon = 975$ was lower than the static pressure at $\epsilon = 800$, an indication that the nozzle flowed full at least to an area ratio of 975. On reading 116, however, the static pressure at $\epsilon = 975$ was slightly higher than the pressure at $\epsilon = 800$; here the flow had separated somewhere between these taps. Closer inspection of the data of reading 116 revealed that the thrust performance was still within the nominal scatter band of the rest of the data.

Nozzle wall temperatures were measured at 12 area ratio locations (table IV). The nozzle wall thermocouples were located on the nozzle outer surface at the same axial stations as the static pressure taps but circumferentially displaced by 90°.

Figures 13 and 14 show typical variations of wall static pressure and wall temperature along the nozzle length.

TABLE III.—NOZZLE WALL STATIC PRESSURES

Reading	Effective combustion chamber total pressure at nozzle entrance, $P_{c,e}$		Propellant mixture ratio, O/F	Expansion area ratio, ϵ									
				12		20		50		100		200	
				Nozzle-wall static pressure, P_s									
	kN/m^2	psia		kN/m^2	psia	kN/m^2	psia	kN/m^2	psia	kN/m^2	psia	kN/m^2	psia
112	2482	360.0	3.84	25.12	3.644	14.02	2.034	5.804	0.8418	2.863	0.4153	1.247	0.1809
113	2461	356.9	4.36	25.58	3.710	14.58	2.114	5.943	.8620	2.912	.4224	1.265	.1835
114	2488	360.9	5.08	26.50	3.843	15.11	2.191	6.138	.8902	3.009	.4364	1.307	.1896
115	2450	355.3	5.49	30.98	4.493	16.38	2.375	6.125	.8883	2.941	.4265	1.285	.1863
116	2482	360.0	2.85	27.80	4.032	14.49	2.101	5.580	.8093	2.679	.3886	1.159	.1681
117	2456	356.2	3.19	28.46	4.128	14.87	2.156	5.685	.8246	2.732	.3963	1.175	.1704
120	2449	355.2	4.30	23.79	3.451	14.87	2.156	5.992	.8690	2.890	.4192	1.258	.1825
121	2482	360.0	4.11	24.02	3.484	15.04	2.181	6.046	.8769	2.911	.4222	1.269	.1841
123	2449	355.2	3.19	21.88	3.173	13.84	2.008	5.637	.8176	2.725	.3952	1.189	.1725
124	2492	361.4	2.78	21.00	3.046	13.42	1.946	5.542	.8038	2.683	.3891	1.178	.7467
125	2441	354.0	3.74	22.23	3.224	13.62	1.975	5.750	.8339	2.805	.4069	1.229	.1783

Reading	Expansion area ratio, ϵ											
	300		388		500		635		800		975	
	Nozzle wall static pressure, P_s											
	kN/m^2	psia	kN/m^2	psia	kN/m^2	psia	kN/m^2	psia	kN/m^2	psia	kN/m^2	psia
112	0.7846	0.1138	0.5694	0.08259	0.4091	0.05933	0.3010	0.04366	0.2136	0.03098	0.1817	0.02636
113	.7950	.1153	.5765	.08361	.4107	.05957	.3049	.04422	.2156	.03127	.1818	.02637
114	.8232	.1194	.5961	.08645	.4249	.06162	.3149	.04567	.2208	.03203	.1820	.02639
115	.8184	.1187	.5942	.08618	.4245	.06157	.3174	.04604	.2226	.03229	.1813	.02629
116	.7281	.1056	.5286	.07667	.3762	.05457	.2899	.04204	.2116	.03069	.2130	.03090
117	.7384	.1071	.5390	.07818	.3869	.05612	.2911	.04222	.2097	.03042	.1809	.02624
120	.7929	.1150	.5743	.08330	.4136	.05998	.3081	.04469	.2209	.03204	.1884	.02732
121	.8026	.1164	.5887	.08538	.4200	.06092	.3119	.04523	.2227	.0323	.1903	.02760
123	.7508	.1089	.5485	.07955	.3940	.05714	.2942	.04267	.2139	.03102	.1882	.02730
124	.7467	.1083	.5458	.07916	.3925	.05692	.2954	.04284	.2149	.03117	.1879	.02725
125	.7743	.1123	.5623	.08156	.4053	.05878	.3023	.04384	.2173	.03152	.1859	.02696

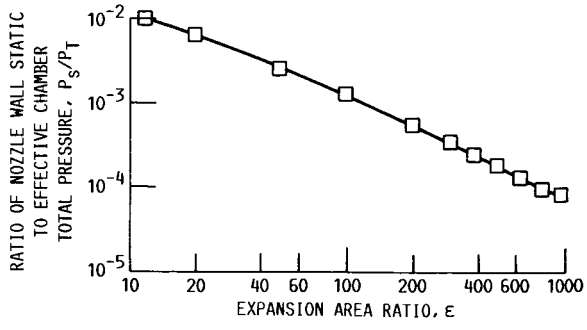

Figure 13.—Nozzle wall static pressure ratio distribution. Reading 120.

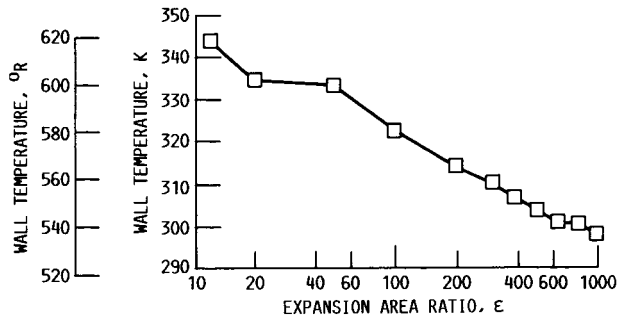

Figure 14.—Nozzle wall temperature distribution. Reading 120.

TABLE IV.—NOZZLE WALL TEMPERATURES

Reading	Effective combustion chamber total pressure at nozzle entrance, $P_{c,e}$		Propellant mixture ratio, O/F	Expansion area ratio, ϵ									
				5.6		12		20		50		100	
				Nozzle wall temperatures									
				K	°R	K	°R	K	°R	K	°R	K	°R
	kN/m^2	psia											
112	2482	360.0	3.84	341.05	613.89	349.25	628.65	333.91	601.03	319.49	575.08	306.65	551.97
113	2461	356.9	4.36	352.08	633.75	361.34	650.42	348.13	626.64	336.09	604.97	322.42	580.35
114	2488	360.9	5.08	366.21	659.18	369.33	664.80	357.51	643.51	346.14	623.06	331.17	596.11
115	2450	355.3	5.49	364.98	656.96	369.68	665.43	361.88	651.39	356.28	641.30	341.84	615.32
116	2482	360.0	2.85	329.63	593.34	340.54	612.98	340.88	613.59	344.44	620.00	337.43	607.37
117	2456	356.2	3.19	333.27	599.89	346.29	623.32	348.13	626.64	353.61	636.49	345.83	622.50
120	2449	355.2	4.30	369.94	665.89	346.89	624.40	336.89	606.41	335.05	603.09	349.38	628.89
121	2482	360.0	4.11	357.53	643.56	348.94	628.10	345.07	621.12	337.31	607.15	321.92	579.46
123	2449	355.2	3.19	332.76	598.97	333.86	600.94	328.58	591.44	322.02	579.64	311.89	561.41
124	2492	361.4	2.78	328.31	590.95	335.14	603.26	331.73	597.12	332.34	598.22	323.23	581.82
125	2441	354.0	3.74	347.34	625.22	342.74	616.93	340.52	612.94	344.95	620.91	334.90	602.82

Reading	Expansion area ratio, ϵ													
	200		300		388		500		635		800		975	
	Nozzle wall temperatures													
	K	°R	K	°R	K	°R	K	°R	K	°R	K	°R	K	°R
112	299.70	539.46	289.98	521.97	296.06	532.90	286.65	515.97	292.78	527.00	285.53	513.95	290.87	523.56
113	312.87	563.17	302.25	544.05	305.08	549.14	295.23	531.42	298.86	537.94	292.08	525.75	295.16	531.28
114	320.81	577.45	310.71	559.28	311.89	561.41	302.02	543.64	303.22	545.80	296.21	533.18	297.39	535.30
115	329.66	593.38	318.62	573.52	318.25	572.85	307.76	553.97	307.53	553.56	300.03	540.06	299.91	539.83
116	329.94	593.89	320.86	577.54	320.28	576.51	310.33	558.60	309.71	557.47	303.42	546.16	303.81	546.86
117	336.60	605.88	326.88	588.39	325.63	586.13	315.68	568.22	314.68	566.42	308.32	554.97	307.76	553.97
120	314.71	566.47	310.43	558.78	307.28	553.10	303.98	547.17	304.16	547.49	300.90	541.62	298.16	536.69
121	312.34	562.22	309.30	556.74	307.11	552.79	304.47	548.04	301.49	542.68	300.39	540.70	297.83	536.09
123	306.85	552.33	305.71	550.28	304.24	547.63	302.61	544.70	300.13	540.24	299.78	539.60	297.52	535.54
124	316.95	570.51	313.80	564.84	310.84	559.51	307.84	554.11	305.05	549.09	304.26	547.67	302.05	543.69
125	326.32	587.37	321.72	579.10	317.92	572.26	313.78	564.80	310.28	558.51	308.92	556.06	305.81	550.46

Summary of Results

An experimental investigation was conducted to determine the thrust performance from a high-area-ratio rocket nozzle. The nozzle had an expansion area ratio of 1030 and a throat diameter of 2.54 cm (1 in.). The tests were performed in the new altitude test capsule at the NASA Lewis Rocket Engine Test Facility. The propellants were gaseous hydrogen and oxygen and the chamber pressure was nominally 2413 kN/m^2 (350 psia).

Several procedural techniques were developed that allowed improved measurements of nozzle performance. The more significant of these were three:

1. Correcting thrust for the aneroid effect: It was discovered that the hermetically sealed load cells in the thrust stand would change their zero point as a result of the altitude transient during the thruster startup. Calibration of this effect allowed its bias to be removed from the run data.

2. Determining the effective chamber pressure: Circumferential and radial pressure distributions have been known to exist across an injector face. Therefore discrete measurements of chamber pressure may not accurately

represent an overall average chamber pressure. The chamber pressure measurement used herein was calibrated by using thrust measurements and thrust coefficient predictions for low-area-ratio nozzles. This calibration was then applied to the test data from the high-area-ratio nozzles.

3. Referencing differential pressure transducers to a vacuum reference tank: An arrangement of automatic shutoff and bypass valves for the nozzle wall static pressure and test capsule pressure transducers allowed the use of very low-range transducers (4 and 34 kN/m^2; 0.6 and 5.0 psia). These transducers were referenced to a very low-pressure vacuum reference tank. Using this system considerably improved the accuracy of these pressure measurements.

Experimental results of atmospheric pressure testing and altitude testing are presented for nozzles with expansion area ratios of 1.4, 428, and 1030. Data are presented in tabular form and also as plots of thrust coefficient as a function of propellant mixture ratio.

National Aeronautics and Space Administration
Lewis Research Center
Cleveland, Ohio, January 29, 1987

References

1. Nickerson, G.R.: The Rao Method Optimum Nozzle Contour Program. Software and Engineering Associates Inc., Carson City, NV, SEA Report 6/82/800.1, June 1982.
2. Bittker, D.A.; and Scullin, V.J.: General Chemical Kinetics Computer Program for Static and Flow Reactions, With Application to Combustion and Shock-Tube Kinetics. NASA TN D-6586, 1972.
3. Evans, R.M.: Boundary Layer Integral Matrix Procedure—User's Manual. (AEROTHERM-UM-75-64, Aerotherm Acurex Corp.; NASA Contract NAS8-30930) NASA CR-144046, 1975.
4. Hendricks, R.C.; Baron, A.K.; and Peller, I.C.: GASP—A Computer Code for Calculating the Thermodynamic and Transport Properties for Ten Fluids: Parahydrogen, Helium, Neon, Methane, Nitrogen, Carbon Monoxide, Oxygen, Fluorine, Argon, and Carbon Dioxide. NASA TN D-7808, 1975.
5. Gordon, S.; and McBride, B.J.: Computer Program for Calculation of Complex Chemical Equilibrium Compositions, Rocket Performance, Incident and Reflected Shocks, and Chapman-Jouguet Detonations. NASA SP-273, 1976.
6. Huff, V.N.; Fortini, A.; and Gordon, S.: Theoretical Performance of JP 4 Fuel and Liquid Oxygen as a Rocket Propellant. II—Equilibrium Composition. NACA RM-E56D23, 1956.
7. Nickerson, G.R.; Coats, D.E.; and Dang, L.D.: Engineering and Programming Manual: Two-Dimensional Kinetic Reference Computer Program (TDK). (SN-63, Software and Engineering Associates; NASA Contract NAS8-35931.) NASA CR-178628, 1985.

1. Report No.	2. Government Accession No.	3. Recipient's Catalog No.
NASA TP-2720		

4. Title and Subtitle	5. Report Date
Experimental Thrust Performance of a High-Area-Ratio Rocket Nozzle	April 1987
	6. Performing Organization Code
7. Author(s)	8. Performing Organization Report No.
Albert J. Pavli, Kenneth J. Kacynski, and Tamara A. Smith	E-3236-1
	10. Work Unit No.
9. Performing Organization Name and Address	11. Contract or Grant No.
National Aeronautics and Space Administration Lewis Research Center Cleveland, Ohio 44135	13. Type of Report and Period Covered Technical Paper
12. Sponsoring Agency Name and Address	14. Sponsoring Agency Code
National Aeronautics and Space Administration Washington, D.C. 20546	

15. Supplementary Notes

Presented at 23rd JANNAF Combustion Meeting, NASA Langley Research Center, October 20–24, 1986.

16. Abstract

An experimental investigation was conducted to determine the thrust performance attainable from high-area-ratio rocket nozzles. A modified Rao-contoured nozzle with an expansion area ratio of 1030 was test fired with hydrogen-oxygen propellants at altitude conditions. The nozzle was also tested as a "truncated" nozzle, at an expansion area ratio of 428. Thrust coefficient and thrust coefficient efficiency values are presented for each configuration at various propellant mixture ratios (oxygen/fuel). Several procedural techniques were developed that allowed improved measurement of nozzle performance. The more significant of these were correcting the thrust for the aneroid effect, determining the effective chamber pressure, and referencing differential pressure transducers to a vacuum reference tank.

17. Key Words (Suggested by Author(s))	18. Distribution Statement
High-area-ratio nozzles; Rocket nozzle performance	Unclassified – unlimited STAR Category 20

19. Security Classif. (of this report)	20. Security Classif. (of this page)	21. No of pages	22. Price*
Unclassified	Unclassified	15	A02

*For sale by the National Technical Information Service, Springfield, Virginia 22161

NASA-Langley, 1987